American Mineralogist, Volume 87, pages 318–326, 2002

Raman spectroscopy of Fe_2O_3 to 62 GPa

SANG-HEON SHIM* AND THOMAS S. DUFFY

Department of Geosciences, Princeton University, Princeton, New Jersey 08544, U.S.A.

ABSTRACT

Raman spectra of Fe_2O_3 were measured to 62 GPa in a diamond anvil cell. All group theoretically predicted Raman-active phonon modes were detected to 54 GPa. In addition, some high-pressure spectra show an IR-active E_u mode (~660 cm^{-1}), possibly induced by surface defects or stress. This mode is related by a factor of two to a mode at 1320 cm^{-1}. The assignment of the 1320 cm^{-1} mode has been controversial (two-magnon scattering or two-phonon scattering), and our observation supports the phonon assignment. All Raman-active phonons show nonlinear pressure-induced shifts. The mode Grüneisen parameters and their logarithmic volume dependences for two low-frequency phonons, A_{1g} and E_g, become negative and infinite, respectively, near 50 GPa as a result of the instability of the corundum structure at this pressure. Using the observed Raman-active phonons together with acoustic phonons previously measured by ultrasonics, and Kieffer's model, we calculate the phonon contribution to the thermodynamic parameters of hematite. Comparison with experimentally measured values allows an estimation of an upper bound to the magnon contribution to the heat capacity at ambient pressure. This increases continuously above the Morin temperature and reaches a maximum at the Néel temperature (~37%). The Raman spectra change dramatically at pressures greater than 54 GPa as indicated by the appearance of new peaks and a significant increase in background. Although direct structural analysis is not possible due to the low signal-to-background ratio and the lack of polarization information, we were able to examine the consistency of our Raman observation with the corundum-to-perovskite phase transformation using the results for an analog system: $MgSiO_3$ ilmenite (ordered corundum type) and perovskite. This analysis shows that observed new features in Fe_2O_3 Raman spectra may not be consistent with the $GdFeO_3$ perovskite structure.

INTRODUCTION

Fe_2O_3 crystallizes in the corundum (α-Al_2O_3) structure at ambient conditions (α-Fe_2O_3, hematite). It is antiferromagnetic below the Morin temperature (T_M = 250 K) and weakly ferromagnetic between 250 K and the Néel temperature (T_N = 950 K) as a result of spin canting. Due to its relatively simple structure and magnetic ordering, hematite has attracted much interest from theorists (e.g., Catti et al. 1995; Punkkinen et al. 1999) and experimentalists (e.g., McQueen and Marsh 1966; Beattie and Gilson 1970; Goto et al. 1982; Yagi and Akimoto 1982; Suzuki et al. 1985; Knittle and Jeanloz 1986; Olsen et al. 1991; Pasternak et al. 1999).

The Raman spectrum of Fe_2O_3 has been measured at both ambient (Hart et al. 1975; Martin et al. 1977; McCarty 1988) and high pressure (Massey et al. 1990a). These studies are in general agreement on the phonon modes but there is controversy over whether the Raman signature at 1320 cm^{-1} originates from two-magnon or two-phonon scattering. Hart et al. (1975) assigned this mode as two-magnon scattering. This idea was supported by Martin et al. (1977) who measured its temperature dependence. However, McCarty (1988) reported that this feature is still observed above the Néel temperature and is related to an IR-active mode in the $Fe_xCr_{2-x}O_3$ solid solution system. Massey et al. (1990a) performed in situ high-pressure Raman experiments to 23 GPa. Using the pressure-induced Raman shift, they showed that the Grüneisen parameter of this line is much lower than the expected value for a magnon (≈3.3) based on Bloch's hypothesis (Bloch 1966). To resolve this question, we have measured the pressure dependence of the 660 cm^{-1} IR-active mode that may be related to the 1320 cm^{-1} mode.

Kieffer (1979a, 1979b, 1979c, 1980, 1982) has shown that using vibrational spectra and an appropriate model for the density of states, thermodynamic properties of a solid can be reliably estimated based purely on phonons. However, the thermodynamic properties of a solid are also affected by electrons and magnons. Hence, Kieffer's model has been most successful for insulators. Hematite is an interesting case because any magnon would also contribute to the thermodynamic properties. By comparing experimentally measured thermodynamic parameters with the value obtained from phonon measurements and Kieffer's model, it is expected that an estimate of the non-phonon contribution may be obtained.

* Present address: Department of Earth and Planetary Science, University of California, Berkeley, CA 94720-4767. E-mail: sangshim@uclink.berkeley.edu

A phase transformation involving a 10–15% volume change was found above 60 GPa by shock wave experiments on Fe_2O_3 (McQueen and Marsh 1966). Reid and Ringwood (1969) extrapolated the shock density to ambient pressure and speculated that the high-pressure phase of Fe_2O_3 could be perovskite based on systematics between volume per formula unit and average octahedral bond length. To accommodate the Fe ion into two different crystallographic sites with different coordination numbers (6 and 8–12), they proposed the existence of two different valence states, i.e., $Fe^{2+}Fe^{4+}O_3$. Subsequently several studies have focused on solving the structure of the high pressure phase (e.g., Yagi and Akimoto 1982; Suzuki et al. 1985; Olsen et al. 1991; Pasternak et al. 1999).

From Mössbauer spectra, Suzuki et al. (1985) concluded that the Fe ion is close to Fe^{2+} rather than Fe^{3+} and in a low spin state. This might imply the existence of Fe^{4+}. Pasternak et al. (1999) investigated the nature of the phase transformation using angle-dispersive X-ray diffraction (XRD), Mössbauer, and resistivity measurements. Their Mössbauer result shows that above 82 GPa only one valence state, Fe^{3+}, exists without magnetism. They claimed that the discrepancy with the earlier Mössbauer study (Suzuki et al. 1985) is due to pressure inhomogeneity in the earlier study. This supports the existence of the Rh_2O_3-II structure that has only one crystallographic cation site and therefore only one cation valence state.

There are few high-pressure Raman measurements of highly absorbing samples (Gillet et al. 1998). In the case of Fe_2O_3, previous Raman work (Massey et al. 1990a) extended only to 23 GPa, well below the phase transformation pressure. Using a new micro-Raman spectroscopy system (LaPlant and Ben-Amotz 1995; Goncharov et al. 1999), we have measured the vibrational spectra of the high pressure phase of Fe_2O_3 to 62 GPa and we examined the nature of the 1320 cm^{-1} mode. We also derived the phonon contribution to the thermodynamic parameters using Kieffer's model (Kieffer 1979c) and estimated an upper bound to the magnon contribution. Group theoretical analysis and the examination of possible structure types for the high-pressure phase are also discussed.

Experimental methods

Pure synthetic Fe_2O_3 (Alfa, purity 99.998%) was used in powder form. The sample quality was confirmed using powder XRD and Raman spectroscopy at ambient conditions. Powder samples were gently pressed between two glass slides and loaded in 100 or 150 μm diameter holes in stainless steel gaskets. Low fluorescence diamond anvils with 300 μm culets were used to compress the sample in a symmetric diamond anvil cell (DAC). Argon was loaded cryostatically as a pressure transmitting medium. In order to prevent heating by the focused incident laser beam, the sample foil was loaded in direct contact with a diamond anvil and spectra were measured from this side (Fig. 1). We also used low laser power (~10–20 mW) to reduce sample heating.

Several ruby chips were loaded at various sample positions for pressure determination using the quasi-hydrostatic ruby scale (Mao et al. 1986) (Fig. 1). All ruby grains were loaded on the opposite side of the sample surface from which we measured vibrational spectra (Fig. 1). Since the sample is opaque, no signal from ruby is observed in our spectra. The homogeneity of the stress condition was confirmed by measuring pressures at different positions across the sample. In general, the pressure difference did not exceed ±1 GPa.

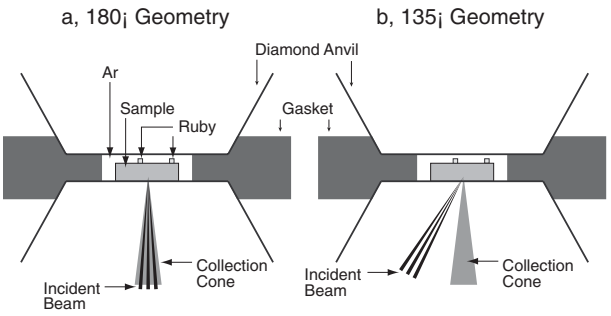

Figure 1. Experimental setup for (**a**) 180° and (**b**) 135° scattering geometries.

The micro-Raman system used in this study consists of a 200 mW Ar-ion laser (514.532 nm), single grating 0.5 m spectrometer, charge-couple device (CCD) detector (1100 × 330 pixels), and holographic optics. Compared to the conventional triple-grating spectrometer, this single-grating spectrometer yields a better signal-to-noise ratio and higher transmission (McCreery 1994). To decrease the diffuse scattering from the highly reflective sample and fluorescence from the diamond anvil, we used a 135° angle between the incident beam and collecting direction (Fig. 1), especially above 50 GPa. At lower pressure we used both 180° and 135° geometries. The focal spot size was 10–20 μm. A detailed description of this type of micro-Raman system can be found in LaPlant and Ben-Amotz (1995), and Goncharov et al. (2000).

A spectral range of 50–2200 cm^{-1} was examined in this study using an 1800 grooves/mm grating. The spectrometer was regularly calibrated using the neon emission spectrum. The precision of the measured frequency is better than ±2 cm^{-1}. A 10 minute exposure time was used at pressures up to 50 GPa. Near and after the phase transformation, the Raman signal decreased significantly and an one-hour exposure was used. Due to the strong diamond Raman mode, the 1300–1500 cm^{-1} spectral range was not examined.

Result and discussion

Raman spectra of α-Fe_2O_3 to 54 GPa

All seven phonon modes predicted by group theory were observed at pressures up to 54 GPa (Figs. 2 and 3). Assignments were made following the polarized single-crystal Raman measurements of Beattie and Gilson (1970). The observed phonon modes show good agreement with previous studies at ambient conditions (Table 1) (Beattie and Gilson 1970; Massey et al. 1990a) and at pressures up to 23 GPa (Figs. 2 and 3) (Massey et al. 1990a).

Up to 50 GPa, the relative intensity of the $A_{1g}(1)$ mode continuously increases compared to other lines: the intensity ratio between the $A_{1g}(1)$ and $E_g(2)$ modes is about one at 0 GPa but fifteen at 50 GPa. Above 50 GPa, a significant intensity de-

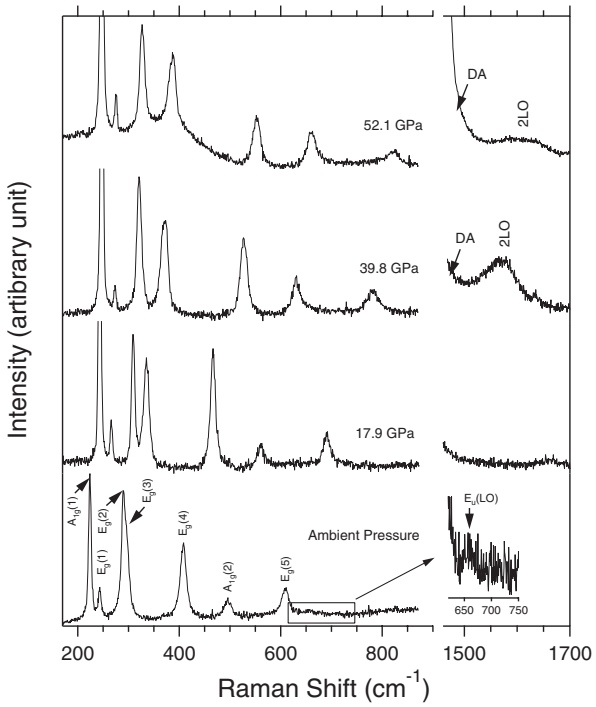

FIGURE 2. Representative Raman spectra of hematite to 52.1 GPa. The spectra are normalized to the intensity of the $E_g(2)$ mode. Raman signal from the diamonds is indicated with "DA." Peak assignment is shown for each phonon mode. The 620–750 cm^{-1} range is shown in the inset to illustrate the observation of Raman-inactive and IR-active E_u (LO) mode.

TABLE 1. Phonon frequencies, ν_{i0}, and their mode Grüneisen parameters, γ_{i0}, at ambient conditions

	Beattie and Gilson (1970)	Massey et al. (1990a)		This study	
	ν_{i0} (cm^{-1})	ν_{i0} (cm^{-1})	γ_{i0}	ν_i (cm^{-1})	γ_{i0}
$A_{1g}(1)$	226	228	0.7(1)	224	0.76(10)
$E_g(1)$	245	246	1.1(1)	243	0.97(13)
$E_g(1)$	293	294	0.6(1)	290	0.45(6)
$E_g(1)$	298	300	1.8(1)	297	1.57(20)
$E_g(1)$	413	412	1.7(1)	408	1.31(16)
$A_{1g}(2)$	500	496	1.7(1)	496	1.27(16)
$E_g(1)$	612	614	2.0(2)	609	1.34(17)
E_u				659	1.24(16)
$2E_u$		1320	1.2(1)	1316	1.29(14)

Notes: The number in parentheses is the estimated uncertainty (1σ). Our error bars are comparable to those reported by Massey et al. (1990a), because, while we have a smaller error on $d\nu/dP$, they did not include the uncertainty in the bulk modulus.

crease for all phonon modes was observed. The higher frequency Raman modes, $E_g(2)$, $E_g(3)$, $E_g(4)$, and $A_{1g}(2)$, exhibit some hysteresis and are shifted to higher frequency during decompression. The observation of features from the high-pressure phase (ν_1 and ν_2 in Fig. 3a) down to 25 GPa during decompression suggests that the metastable persistence of high-pressure phase may contribute to this hysteresis.

We performed polynomial fits to the Raman frequencies as a function of pressure by combining our data with that of Massey et al. (1990a). The data points obtained during decompression were not included. All hematite phonon modes show a significant nonlinear pressure dependence (Fig. 3), which was not detected by the earlier measurements (Massey et al. 1990a).

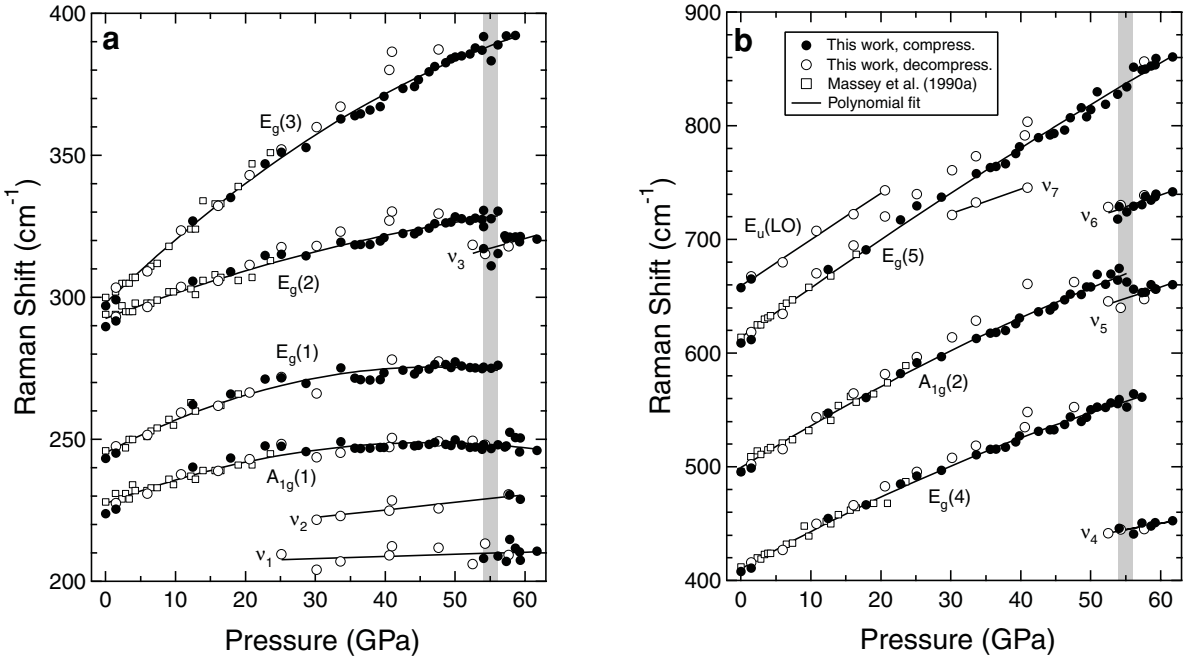

FIGURE 3. Pressure-induced frequency shifts of phonon modes. Solid circles indicates data measured during compression and open circles are data measured during decompression. The measurements of Massey et al. (1990a) are shown by open squares. The solid lines are polynomial fits to the data. Polynomial fits are required due to the significant nonlinearity of all modes. New modes for the high-pressure phase are assigned as ν_i (i = 1~7) in order of lowest wave number. The pressure range where we observed changes in the Raman spectrum is indicated by gray shading.

The χ^2 value of the least squares fit decreases by 35–50% by introducing the quadratic term. While in most high pressure Raman spectra the pressure-induced phonon shifts are well described by linear functions of pressure, nonlinear behavior has been observed for some materials (Williams et al. 1987; Jephcoat et al. 1988; Hofmeister et al. 1989; Chopelas 1990a; Chopelas 1990b; Chopelas and Hofmeister 1991; Hofmeister 1997).

There has been considerable controversy regarding whether the mode observed at 1320 cm^{-1} originates from a secondary magnon-photon interaction (Hart et al. 1975; Martin et al. 1977) or a secondary phonon-photon interaction (McCarty 1988; Massey et al. 1990a). Recent studies (McCarty 1988; Massey et al. 1990a) prefer the latter assignment based on observations for the $Fe_xCr_{2-x}O_3$ solid solution system, Bloch's 10/3 theorem, and isotopically substituted samples.

Bloch's (1966) hypothesis predicts that the mode Grüneisen parameter for magnons, γ_{magnon}, should be much greater than that for phonons and close to 10/3 based on a variety of empirical trends. However, at that time the accessible pressure range was limited. Thus far, few observations have been reported for the behavior of magnons at pressures greater than 10 GPa (e.g., Massey et al. 1990b; Massey et al. 1992; Struzhkin et al. 1993a; Struzhkin et al. 1993b; Rosenblum and Merlin 1999). Massey et al. (1990b) reported $\gamma_{magnon} = 3.5 \pm 0.1$ for NiO at 0–30 GPa that seems to obey Bloch's hypothesis. However, γ_{magnon} for CoO at 0–17 GPa was reported to be only 2.7 ± 0.2 (Struzhkin et al. 1993a). By using an updated bulk modulus, K_{T0}, for NiO, Struzhkin et al. (1993b) argued that the γ_{magnon} should be 2.3–2.6. Moreover, by reviewing available data, they showed that γ_{magnon} ranges between 1.6–3.3 and may be material dependent in contrast to Bloch's hypothesis. These recent results based on higher pressure measurements indicate that the 10/3 empirical ratio may not be universal and could be material dependent. Thus, Bloch's hypothesis cannot be considered conclusive in distinguishing a magnon from a phonon.

We observed the 1320 cm^{-1} mode at high pressures (Figs. 2 and 4). A strong nonlinear pressure dependence is observed above 30 GPa. The mode then disappears when the phase transformation occurs at 54 GPa. We also observed a weak and broad feature at 658 cm^{-1} at 0 and 1.5 GPa during compression and 1.5–20.6 GPa during decompression, which has not been reported previously (Figs. 2 and 3b). This mode shows good agreement with the IR active E_u(LO) mode at 662 cm^{-1} observed in IR measurements (Onari et al. 1977) and at 660–690 cm^{-1} for Raman measurements in solid solutions $Fe_xCr_{2-x}O_3$ ($0 \le x \le 2$) (McCarty and Boehme 1989). Thus, this feature may be assigned as an IR active E_u(LO) mode. However, this mode is not group theoretically allowed in Raman spectra and has not been reported for the end-member. This could appear due to a strong resonance on the surface where the solid may not have the complete symmetry of the bulk structure or due to defects in the structure induced by stress (McCarty and Boehme 1989). The weak and broad appearance of this peak is consistent with these possibilities. However, according to group theory, its first overtone ($660 \times 2 = 1320$ cm^{-1}) is Raman active (McCarty 1988).

In our study, the frequencies of these two modes are related by a factor of very nearly two at ambient and high pressures (Fig. 4). Their mode Grüneisen parameters are also identical within uncertainty (1.24 ± 0.16 for 658 cm^{-1} and 1.29 ± 0.14 for 1320 cm^{-1}). These observations support the conclusions of McCarty (1988) and Massey et al. (1990a) that the 1320 cm^{-1} mode is from a second order phonon-photon interaction, not from a second order magnon-photon interaction.

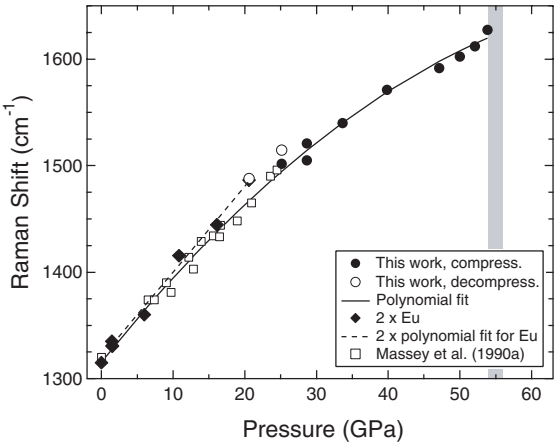

FIGURE 4. Pressure induced shift of 1320 cm^{-1} mode. Notation is the same as in Figure 3. The solid diamonds and dashed line shows twice the frequency of the E_u(LO) mode.

Massey et al. (1990a) proposed that the two magnon scattering is observed at ~1525 cm^{-1} at 80–525 K and ambient pressure based on isotope substitution and temperature dependence studies. However, they were not able to observe this mode at high pressures because of its weak signal. In our experiment, this mode was also not detected. This may be due to both the weak signal and the existence of background structure near this frequency range from the diamond anvils.

Magnon contribution to thermodynamics of α-Fe_2O_3

One of the important thermodynamic parameters for characterizing high *P-T* behavior is the Grüneisen parameter (Stacey 1992; Anderson 2000). By measuring the volume dependence of the vibrational frequency, one can obtain a Grüneisen parameter for each phonon mode. The mode Grüneisen parameters, γ_i, for hematite were calculated using the polynomial fits and the following equation:

$$\gamma_i = -\frac{d\ln \nu_i}{d\ln V} = \frac{K_T}{\nu_i}\left(\frac{d\nu_i}{dP}\right) \quad (1)$$

where ν_i is the frequency of the *i*th phonon mode, *V* is the volume, K_T is the isothermal bulk modulus at a given pressure, and ν and $d\nu/dP$ are obtained from this study. K_{T0} has been measured by several static compression studies (Bassett and Takahashi 1974; Wilburn and Bassett 1978; Sato and Akimoto 1979; Finger and Hazen 1980; Olsen et al. 1991) and can be derived from K_{S0} measured by an ultrasonic study (Liebermann and Schreiber 1968) with results ranging from 178 GPa to 228

GPa. We used K_{T0} = 202.66 GPa derived from ultrasonic measurements and assumed an uncertainty of ±20 GPa.

In order to calculate the average of the mode Grüneisen parameters, $\bar{\gamma}$, one has to weight each mode by the heat capacity for that mode. We used a separate optic continuum for each phonon as described by Xu et al. (1995) and used different weighting factors for acoustic and optic phonons. This yields $\bar{\gamma}_0$ =1.233 ± 0.140. Using the same weighting factor for all optic phonons based on one continuum optic phonon distribution does not significantly change this result. The optic $\bar{\gamma}_0$ is 1.227 ± 0.140, which indicates that the acoustic phonon contribution to the overall thermodynamic properties is negligible.

The average γ can also be calculated using the following thermodynamic relationship:

$$\gamma_{th} = \frac{\alpha K_S}{\rho C_P} \tag{2}$$

where ρ is the density, α is the thermal expansivity (Haas 1988), K_S is the adiabatic bulk modulus (Liebermann and Schreiber 1968), and C_P is the isobaric heat capacity (Chase 1998). The calculated value is 1.51 ± 0.18 that is significantly higher than the result from our Raman measurements. The value from Raman measurement is based on phonons only, whereas the value used for the thermodynamic γ calculation includes all contributions to γ.

We calculated the mode and average γ values at high pressures using our polynomial fits (Fig. 5a). Except for the $E_g(5)$ mode, the mode γ values decrease with pressure for all modes. The mode γ values of $A_{1g}(1)$ and $E_g(1)$ become negative near 50 GPa. The volume dependence of a mode γ, q_i, can also be calculated as follows (Hofmeister et al. 1989):

$$q_i = \frac{d\ln\gamma_i}{d\ln V} = \gamma_i - K'_T - \frac{K_T^2}{\gamma_i \nu_i}\left(\frac{d^2\nu_i}{dP^2}\right) \tag{3}$$

where K'_T is the pressure derivative of bulk modulus at a given pressure (we used K'_{T0} = 4), and $d^2\nu_i/dP^2$ is obtained from our Raman measurement. The result is shown in Figure 5b. The mode q values for $A_{1g}(1)$, $E_g(1)$, and $E_g(3)$ increase strongly and become infinite near 50 GPa. The decrease of γ and the increase of q due to mode softening can be interpreted as an indication of structural instability near the phase boundary. A negative mode γ has also been observed near wurtzite-B1 phase boundary of BeO at high pressure, for example (Jephcoat et al. 1988).

The phonon contribution to thermodynamic properties such as heat capacity, C_V, and entropy, S, can be calculated from the phonon density of states, following Kieffer (1979c). Acoustic phonon frequencies are obtained from ultrasonic measurements (Liebermann and Schreiber 1968). One compressional and two shear modes were calculated using v_P = 7.9012 km/sec and v_S = 4.1626 km/sec, respectively, assuming the two shear modes are identical. The Grüneisen parameters were calculated to be γ_P = 1.53 and γ_S = 0.64.

The optic phonon continuum from 177 to 614 cm^{-1} was obtained from our Raman measurement results (Table 1). The total number of phonons for the corundum structure is eighteen (Table 2). One could also include six IR active phonons measured by Onari et al. (1977). Since their mode γ values are not known, we do not include these phonons. However, IR-active phonons generally lie within or close to the optic continuum calculated from Raman-active modes. The frequencies of the inactive modes are not known. However, since the co-

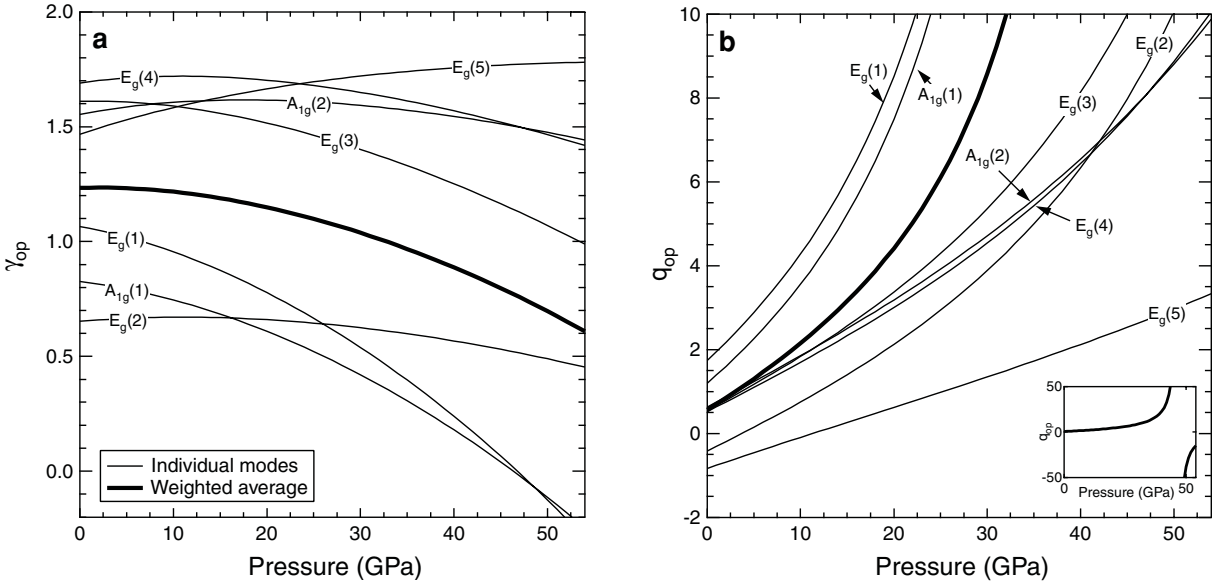

FIGURE 5. (**a**) Grüneisen parameter, γ, and (**b**) its logarithmic volume derivative, q, for each phonon mode and their weighted average as a function of pressure. The inset in (**b**) illustrates the singularity of q for the average.

TABLE 2. Group theoretical analysis of possible structure types

Structure type	Γ (acoustic)	Γ (Raman)	Γ (IR)	Γ (inactive)
corundum (D^6_{3d})	$A_{2u} + E_u$	$2A_{1g} + 5E_g$	$2A_{2u} + 4E_u$	$3A_{2g} + 2A_{1u}$
Rh_2O_3-II (D^{14}_{2h})	$B_{1u} + B_{2u} + B_{3u}$	$7A_g + 8B_{1g} + 8B_{2g} + 7B_{3g}$	$7B_{1u} + 7B_{2u} + 6B_{3u}$	$7A_u$
$GdFeO_3$ (D^{16}_{2h})	$B_{1u} + B_{2u} + B_{3u}$	$7A_g + 7B_{1g} + 5B_{2g} + 5B_{3g}$	$7B_{1u} + 9B_{2u} + 9B_{3u}$	$8A_u$

Note: The space group for each structure is shown in parenthesis.

rundum structure is expected to have lattice modes only but no internal mode (Iishi 1978), which normally exists at much higher frequency range, it is expected that all inactive phonons will originate from lattice vibration and lie near or within the calculated optic continuum for the Raman active phonons.

The calculated isochoric heat capacity, C_V, using Kieffer's model is transformed to the isobaric heat capacity, C_P, using following equation:

$$C_P = C_V(1 + \alpha\gamma T). \quad (4)$$

The calculated result is shown together with the calorimetrically measured value (Chase 1998) in Figure 6a. A discrepancy starts to appear near the Morin temperature, T_M, where the spins become canted resulting in weak ferromagnetism. Up to the Néel temperature, T_N, the discrepancy increases continuously and finally reaches 37%. After T_N, the measured heat capacity decreases and eventually it reaches a plateau near 1000 K. The solid line shows the pure phonon contribution to C_P. The difference between these two is taken to correspond to an upper bound to the magnon contribution.

Ulbrich and Waldbaum (1976) discussed the contribution to thermodynamic parameters from various sources. For materials that show magnetic transformations, two apparent effects on C_P have been observed: an λ-type C_P change near the transition temperature and a background contribution that can be observed at high temperature when the magnetic moments are completely disordered (Ulbrich and Waldbaum 1976). The second effect for 3*d* transition elements can be calculated empirically as follows:

$$S_{magnon} = nR\ln(2S + 1) \quad (5)$$

where n is the number of spin polarized atoms in a unit-cell, R is the gas constant, and S is the spin quantum number. S_{magnon} is calculated for hematite using $n = 2$ and $S = 5/2$ (Ulbrich and Waldbaum 1976) (Fig. 6b). The calculated entropy, including the phonon and magnon effects (from equation 5), shows good agreement with experimental measurement at high temperature. The remaining 4% difference may be explained by contributions from the λ-type C_P change as well as other factors including defects and anharmonicity.

Pressure-induced phase transformation

Between 54 and 56 GPa the $E_g(1)$, $E_g(2)$, and $E_g(4)$ modes disappear and six new features appear at 210, 230, 320, 440, 650, and 740 cm^{-1} ($\nu_1 \sim \nu_6$ in Figs. 2, 3, and 7). A new mode is also observed at 730 cm^{-1} (ν_7) only upon decompression. In contrast to the hematite Raman spectrum, the spectrum of the high-pressure phase is extremely weak and the relative strength

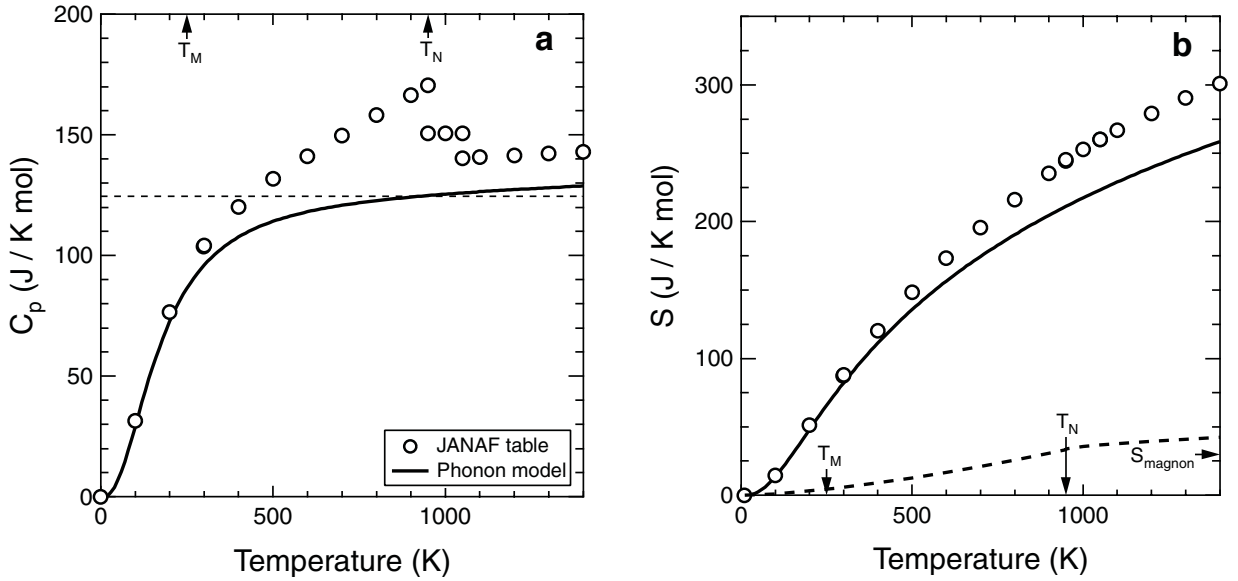

FIGURE 6. (**a**) Isobaric heat capacity, C_P, and (**b**) entropy, S, from calorimetry (open circles; Chase 1998) and from Kieffer's model using phonons measured in this study (solid line). Morin temperature (T_M), Néel temperature (T_N), and empirical calculation of magnon entropy contribution, S_{magnon}, are shown with arrows. The Dulong-Petit limit is shown by a dashed line in (**a**). The difference between the calorimetrically measured and calculated entropy is shown by a dashed line in (**b**) to compare with the empirical calculation for the magnon contribution.

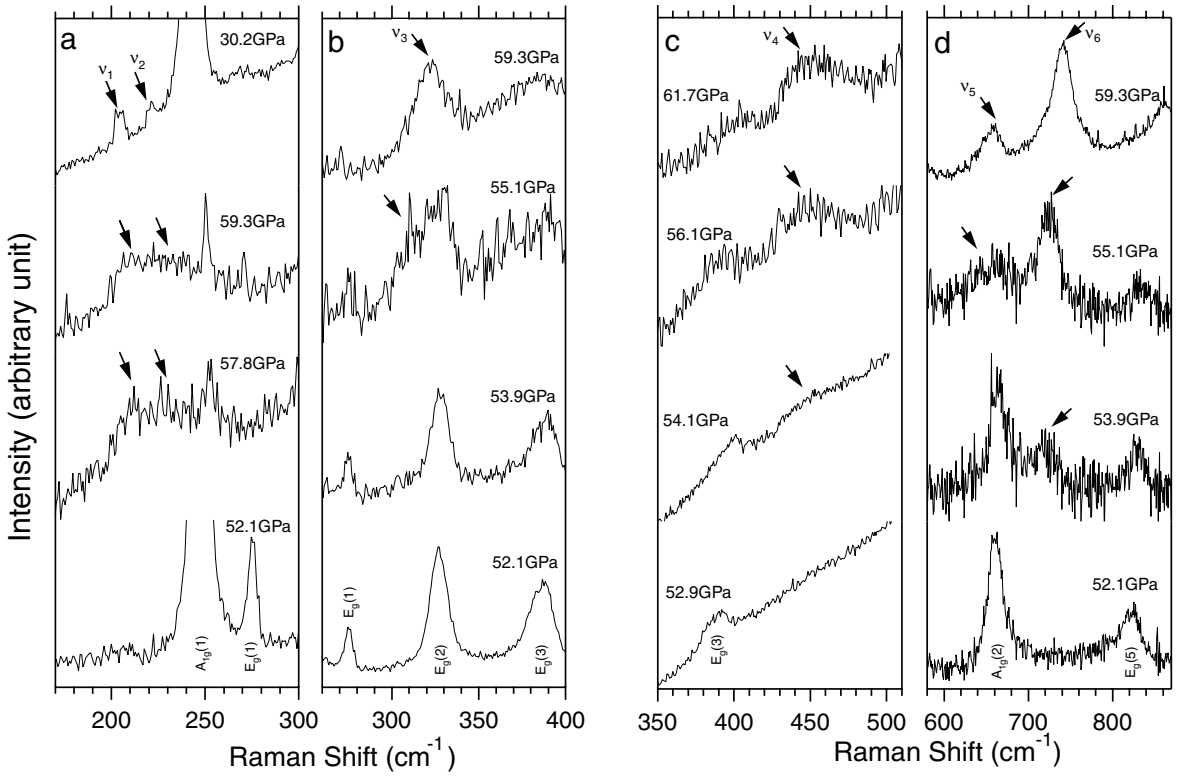

FIGURE 7. Raman spectra of Fe_2O_3 showing evidence for high-pressure phase transformation for (**a**) 170–300 cm^{-1}, (**b**) 260–400 cm^{-1}, (**c**) 350–510 cm^{-1}, and (**d**) 590–835 cm^{-1}. The new peaks are highlighted by arrows. Assignments for the low-pressure phase are given. In (**a**) 30.2 GPa spectrum was obtained during decompression.

of the background increases. The peaks are also much broader than those of hematite. The low signal-to-background ratio for this material is similar to what we observe with our system for the Raman signal of metals such as iron and cobalt. This is consistent with the decrease of electric resistivity of Fe_2O_3 across the phase transformation (Knittle and Jeanloz 1986; Pasternak et al. 1999).

Unlike previous studies that found a broad coexistence region between the low and high pressure phases (45–60 GPa) in XRD patterns (Suzuki et al. 1985; Olsen et al. 1991; Pasternak et al. 1999), we were able to determine the phase boundary over a narrow interval (between 54–56 GPa) on compression using Raman spectroscopy. This may be due to the extremely weak signal of the high pressure phase compared to that of the low-pressure phase: even if the high pressure phase exists at lower pressure together with the corundum phase, the Raman signal from the low-pressure phase dominates. If this is the case, our Raman boundary may be the last point where the low-pressure phase exists or an upper bound to the phase boundary.

Two new low-frequency modes, ν_1 and ν_2, and one new high-frequency mode, ν_7, from the high-pressure phase persist down to 25 GPa upon decompression. In addition, the high frequency hematite modes lie 10–20 cm^{-1} higher after being subjected to transformation back from the high-pressure phase. These observations imply that some of the distortions induced by the phase transformation still survive metastably in the stability field of the low-pressure phase.

Several XRD studies showed that the structure of the high-pressure phase could be either $GdFeO_3$ perovskite (Yagi and Akimoto 1982) or Rh_2O_3-II (Pasternak et al. 1999). For each phase, we calculated the number of normal modes and their activities for IR and Raman using group theory (Table 2). A total of thirty modes are Raman active for the Rh_2O_3-II structure and twenty four modes are Raman active for the $GdFeO_3$ structure. However, we were able to observe only nine modes, so this information cannot be used to distinguish between the two possible structures.

These two structures belong to the same point group (D_{2h}), so the differences in vibrational spectra may be subtle. The only difference in Raman active modes is that the inactive mode, A_{2g}, for the corundum structure becomes Raman active, $3B_{1g} + 3B_{2g}$, for Rh_2O_3-II structure, whereas all Raman active modes for $GdFeO_3$ structure originate only from Raman active modes for the corundum structure. This information may be useful if one can characterize whether or not a new mode is related to the mode of the low pressure phase. However, without the peak assignments for the new modes, the structure of the high-pressure phase remains ambiguous.

The vibrational spectrum of well-characterized analog system have been used to interpret the spectrum of powder samples (Williams et al. 1987; Hofmeister 1993; McMillan and Ross 1987). Thus far there is no reported vibrational spectrum for

the Rh_2O_3-II structure. In addition, we are not aware of any other single cation sesquioxide that has both the corundum and perovskite structure. However, the $MgSiO_3$ system has both the ordered corundum structure (Horiuchi et al. 1982), i.e., ilmenite, and orthorhombic perovskite structure (Horiuchi et al. 1987). Raman spectra have been measured for $MgSiO_3$ ilmenite (Ross and McMillan 1984; Reynard and Rubie 1996) and orthorhombic perovskite (Williams et al. 1987; Gillet et al. 2000). However, no polarized single crystal measurement has been performed for these materials. Using systematics of isomorphs, tentative assignments have been reported (McMillan and Ross 1987; Williams et al. 1987; Gillet et al. 2000).

A comparison of Raman spectra in the $MgSiO_3$ and Fe_2O_3 systems is shown in Figure 8. The correlation between ilmenite and corundum is indicated by dashed lines following the study by McMillan and Ross (1987). For guidance, we also show the relation of low-pressure phase modes to high-pressure phase modes and peak splittings in the Fe_2O_3 system using short dashed lines. It is evident that the highest frequency ilmenite mode disappears in the Raman spectrum of perovskite. However, in the Fe_2O_3 system, the highest frequency mode, $E_g(5)$, still survives after the phase transformation. We also highlighted other modes that disappear after the phase transformation by arrows in Figure 8. However, the related modes in ilmenite still exist in the perovskite Raman spectrum. These differences may indicate that the observed Raman spectrum of the high pressure phase of Fe_2O_3 is inconsistent with the signature of the corundum-to-perovskite phase transformation. This agrees with the recent Mössbauer result for the high pressure phase of Fe_2O_3 (Pasternak et al. 1999) where only one oxidation state of Fe was observed that is not consistent with the perovskite structure. However, our conclusions must remain tentative, as we have no information about the correlation between the Fe_2O_3 system and the corundum to Rh_2O_3-II phase transformation.

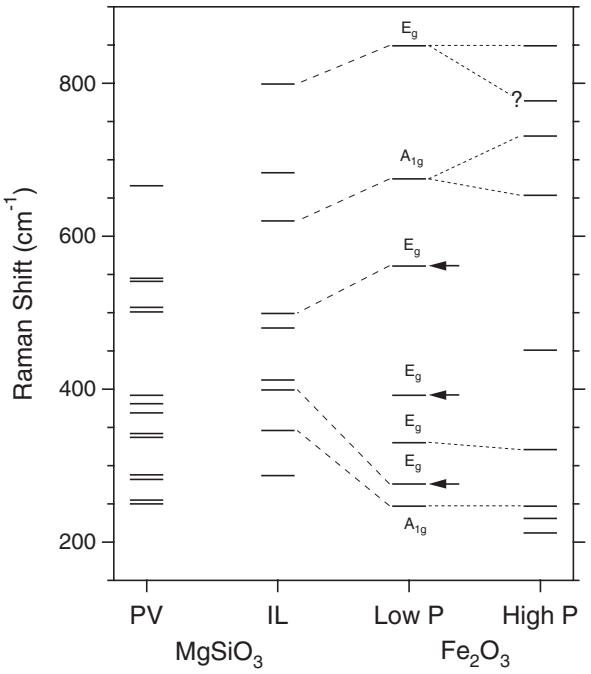

FIGURE 8. Raman modes before and after the phase transformation for Fe_2O_3 at 55 GPa. Modes for $MgSiO_3$ ilmenite and perovskite phases are shown for comparison. Group theoretical correlation between $MgSiO_3$ ilmenite and Fe_2O_3 corundum phases are shown by dashed lines. Peak splitting and continuation through phase transformation in Fe_2O_3 system is denoted by short dashed lines. The modes that disappear after the phase transformation are highlighted by arrows. "?" denotes a new mode observed only during decompression.

It is also worthwhile to revisit the prediction of an orthorhombic perovskite structure for the high-pressure phase of Fe_2O_3 by Reid and Ringwood (1969). They used the relationship between volume per formula unit and average octahedral bond length at ambient pressure. However, at that time the Rh_2O_3-II structure was not known. If one plots the volume of Fe_2O_3 with the Rh_2O_3-II structure on their plot calculated using the result of Shannon and Prewitt (1970), the volume lies slightly lower than that of the B-rare earth type structure (Cromer 1957) but higher than that of perovskite. Because the volume of corundum is much greater than those of the Rh_2O_3-II and perovskite phases, the Rh_2O_3-II structure should be considered equally plausible as the perovskite structure on the basis of volume considerations. The predictability of these systematics is limited, however, as Reid and Ringwood (1969) predicted that $MgSiO_3$ ilmenite would be stable between 60 and 120 GPa. However, it has since been shown that the perovskite structure is stable for that pressure range (Liu 1975; Fiquet et al. 2000; Shim et al. 2001).

ACKNOWLEDGMENTS

We thank J. Badro, C. Merzbacher, and M. Pasternak for helpful discussion and comments. This work was supported by the NSF and the David and Lucile Packard foundation.

REFERENCES CITED

Anderson, O.L. (2000) The Grüneisen ratio for the last 30 years. Geophysical Journal International, 143, 279–294.

Bassett, W.A. and Takahashi, T. (1974) X-ray diffraction studies up to 300 kbar. In R.H. Wentorf Ed., Advances in high pressure research, p. 165–247. Academic Press, New York.

Beattie, I.R. and Gilson, T.R. (1970) The single-crystal Raman spectra of nearly opaque materials—iron (III) oxide and chromium (III) oxide. Journal of the Chemical Society, A5, 980–986.

Bloch, D. (1966) The 10/3 law for the volume dependence of superexchange. Journal of Physics and Chemistry of Solids, 27, 881–885.

Catti, M., Valerio, G., and Dovesi, R. (1995) Theoretical study of electric, magnetic, and structural properties of α-Fe_2O_3 (hematite). Physical Review B: Condensed Matter, 51, 7441–7450.

Chase, Jr., M.W. (1998) NIST-JANAF thermochemical tables. American Institute of Physics for the National Institute of Standards and Technology, New York.

Chopelas, A. (1990a) Thermal expansion, heat capacity, and entropy of MgO at mantle pressures. Physics and Chemistry of Minerals, 17, 142–148.

———(1990b) Thermal properties of forsterite at mantle pressures derived from vibrational spectroscopy. Physics and Chemistry of Minerals, 17, 149–156.

Chopelas, A. and Hofmeister, A.M. (1991) Vibrational spectroscopy of aluminate spinels at 1 atm and of $MgAl_2O_4$ to over 200-kbar. Physics and Chemistry of Minerals, 18, 279–293.

Cromer, D.T. (1957) The crystal structure of monoclinic Sm_2O_3. Journal of Physical Chemistry, 61, 753–755.

Finger, L.W., and Hazen, R.M. (1980) Crystal structure and isothermal compression of Fe_2O_3, Cr_2O_3, and V_2O_3 to 50 kbars. Journal of Applied Physics, 51, 5362–5367.

Fiquet, G., Dewaele, A., Andrault, D., Kunz, M., and Bihan, T.L. (2000) Thermoelastic properties and crystal structure of $MgSiO_3$ perovskite at lower mantle pressure and temperature conditions. Geophysical Research Letters, 27, 21–24.

Gillet, P., Daniel, I., Guyot, F., Matas, J., and Chervin, J.-C. (2000) A thermodynamic model for $MgSiO_3$-perovskite derived from pressure, temperature and volume dependence of the Raman mode frequencies. Physics of the Earth and

Planetary Interiors, 117, 361–384.
Gillet, P., Hemley, R.J., and McMillan, P.F. (1998) Vibrational properties at high pressures and temperature. In R.J. Hemley, Ed., Ultrahigh-pressure mineralogy, volume 37 of Reviews in Mineralogy, p. 525–590. Mineralogical Society of America.
Goncharov, A.F., Struzhkin, V.V., Mao, H.-K., and Hemley, R.J. (1999) Raman spectroscopy of dense H_2O and the transition to symmetric hydrogen bonds. Physical Review Letters, 83, 1998–2001.
Goncharov, A.F., Struzhkin, V.V., Hemley, R.J., Mao, H.-K., and Liu, Z. (2000) New techniques for optical spectroscopy at ultrahigh pressures. In M.H. Manghnani, W.J. Nellis, and M.F. Nicol, Eds., Science and technology of high pressure, p. 90–95. University Press, India.
Goto, T., Sato, J., and Syono, Y. (1982) Shock-induced spin-pairing transition in Fe_2O_3 due to the pressure effect on the crystal field. In S. Akimoto and M.H. Manghnani, Eds., High-pressure research in geophysics, p. 595–609. Center for Academic Publications Japan, Tokyo.
Haas, J.L. (1988) Recommended standard electrochemical potentials and fugacities of oxygen for solid buffers and thermodynamic data in the system iron-silicon-oxygen, nickel-oxygen, and copper-oxygen, preliminary report of January 17, 1988 to the CODATA task group on chemical thermodynamic tables. U.S. Geological Survey.
Hart, T.R., Adams, S.B., and Temkin, H. (1975) Raman scattering from phonons and magnons in α-Fe_2O_3. In M. Balkanski, R.C.C. Leite, and S.P.S. Porto, Eds., Proceedings of the third international conference on light scattering in solids, p. 259–263. Wiley, Campinas, Brazil.
Hofmeister, A.M. (1993) IR reflectance spectra of natural ilmenite: comparison with isostructural compounds and calculation of thermodynamic properties. European Journal of Mineralogy, 5, 281–295.
———(1997) IR spectroscopy of alkali halides at very high pressures: calculation of equations of state and of the response of bulk moduli to the B1-B2 phase transition. Physical Review B: Condensed Matter, 56, 5835–5855.
Hofmeister, A.M., Xu, J., Mao, H.-K., Bell, P.M., and Hoering, T.C. (1989) Thermodynamics of Fe-Mg olivines at mantle pressures: mid- and far-infrared spectroscopy at high pressure. American Mineralogist, 74, 281–306.
Horiuchi, H., Hirano, M., Ito, E., and Matsui, Y. (1982) $MgSiO_3$ (ilmenite-type) single crystal X-ray diffraction study. American Mineralogist, 67, 788–793.
Horiuchi, H., Ito, E., and Weidner, D.J. (1987) Perovskite-type $MgSiO_3$: Single-crystal X-ray diffraction study. American Mineralogist, 72, 357–360.
Iishi, K. (1978) Lattice dynamics of corundum. Physics and Chemistry of Minerals, 3, 1–10.
Jephcoat, A.P., Hemley, R.J., Mao, H.-K., Cohen, R.E., and Mehl, M.J. (1988) Raman spectroscopy and theoretical modeling of BeO at high pressure. Physical Review B: Condensed Matter, 37, 4727–4734.
Kieffer, S.W. (1979a) Thermodynamics and lattice vibrations of minerals: 1. mineral heat capacities and their relationships to simple lattice vibrational models. Reviews of Geophysics and Space Physics, 17, 1–19.
———(1979b) Thermodynamics and lattice vibrations of minerals: 2. vibrational characteristics of silicates. Reviews of Geophysics and Space Physics, 17, 20–34.
———(1979c) Thermodynamics and lattice vibrations of minerals: 3. lattice dynamics and an approximation for minerals with application to simple substances and framework silicates. Reviews of Geophysics and Space Physics, 17, 35–59.
———(1980) Thermodynamics and lattice vibrations of minerals: 4. application to chain and sheet silicates and orthosilicates. Reviews of Geophysics and Space Physics, 18, 862–886.
———(1982) Thermodynamics and lattice vibrations of minerals: 5. applications to phase equilibria, isotopic fractionation, and high-pressure thermodynamic properties. Reviews of Geophysics and Space Physics, 20, 827–849.
Knittle, E. and Jeanloz, R. (1986) High-pressure electrical resistivity measurements of Fe_2O_3: comparison of static-compression and shock-wave experiments to 61 GPa. Solid State Communications, 58, 129–131.
LaPlant, F. and Ben-Amotz, D. (1995) Design and construction of a microscope-based Raman system. Review of Scientific Instruments, 66, 3537–3544.
Liebermann, R.C. and Schreiber, E. (1968) Elastic constants of polycrystalline hematite as a function of pressure to 3 kilobars. Journal of Geophysical Research, 73, 6585–6590.
Liu, L.-G. (1975) Post-oxide phases of forsterite and enstatite. Geophysical Research Letters, 2, 417–419.
Mao, H.-K., Xu, J., and Bell, P.M. (1986) Calibration of the ruby pressure gauge to 800 kbar under quasihydrostatic conditions. Journal of Geophysical Research, 91, 4673–4676.
Martin, T.P., Merlin, R., Huffman, D.R., and Cardona, M. (1977) Resonant two magnon Raman scattering in α-Fe_2O_3. Solid State Communications, 22, 565–567.
Massey, M.J., Baier, U., Merlin, R., and Weber, W.H. (1990a) Effects of pressure and isotopic substitution on the Raman spectrum of α-Fe_2O_3: identification of two-magnon scattering. Physical Review B: Condensed Matter, 41, 7822–7827.
Massey, M.J., Chen, N.H., Allen, J.W., and Merlin, R. (1990b) Pressure dependence of two-magnon Raman scattering in NiO. Physical Review B: Condensed Matter, 42, 8776–8779.
Massey, M.J., Merlin, R., and Girvin, S.M. (1992) Raman scattering in $FeBO_3$ at high pressures: phonon coupled to spin-pair fluctuations and magnetodeformation potentials. Physical Review Letters, 69, 2299–2302.
McCarty, K.F. (1988) Inelastic light scattering in α-Fe_2O_3: phonon vs magnon scattering. Solid State Communications, 68, 799–802.
McCarty, K.F. and Boehme, D.R. (1989) A Raman study of the systems $Fe_{3-x}Cr_xO_4$ and $Fe_{2-x}Cr_xO_3$. Journal of Solid State Chemistry, 79, 19–27.
McCreery, R.L. (1994) CCD array detectors for multi-channel Raman spectroscopy. In J. V. Sweedler, K.L. Ratzlaff, and M.B. Denton, Eds., Charge transfer devices in spectroscopy, chapter 7, p. 227–279. VCH publishers, New York.
McMillan, P.F. and Ross, N.L. (1987) Heat capacity calculations for Al_2O_3 corundum and $MgSiO_3$ ilmenite. Physics and Chemistry of Minerals, 14, 225–234.
McQueen, R.G. and Marsh, S.P. (1966) Handbook in physical constants. Geological Society of America.
Olsen, J.S., Cousins, C.S.G., Gerward, L., Jhans, H., and Sheldon, B.J. (1991) A study of the crystal structure of Fe_2O_3 in the pressure range up to 65 GPa using synchrotron radiation. Physica Scripta, 43, 327–330.
Onari, S., Arai, T., and Kudo, K. (1977) Infrared lattice vibrations and dielectric dispersion in α-Fe_2O_3. Physical Review B: Condensed Matter, 16, 1717–1721.
Pasternak, M.P., Rozenberg, G.K., Machavariani, G.Y., Naaman, O., Taylor, R.D., and Jeanloz, R. (1999) Breakdown of the Mott-Hubbard state in Fe_2O_3: a first-order insulator-metal transition with collapse of magnetism at 50 GPa. Physical Review Letters, 82, 4663–4666.
Punkkinen, M.P.J., Kokko, K., Hergert, W., and Vayrynen, I.J. (1999) Fe_2O_3 within the LSDA+U approach. Journal of Physics: Condensed Matter, 11, 2341–2349.
Reid, A.F. and Ringwood, A.E. (1969) High-pressure scandium oxide and its place in the molar volume relationships of dense structures of M_2X_3 and ABX_3 type. Journal of Geophysical Research, 74, 3238–3252.
Reynard, B. and Rubie, D.C. (1996) High-pressure, high-temperature Raman spectroscopic study of ilmenite-type $MgSiO_3$. American Mineralogist, 81, 1092–1096.
Rosenblum, S.S. and Merlin, R. (1999) Resonant two-magnon Raman scattering at high pressures in the layered antiferromagnetic $NiPS_3$. Physical Review B: Condensed Matter, 59, 6317–6320.
Ross, N.L. and McMillan, P.F. (1984) The Raman-spectrum of $MgSiO_3$ ilmenite. American Mineralogist, 69, 719–721.
Sato, Y. and Akimoto, S. (1979) Hydrostatic compression of four corundum-type compounds: α-Al_2O_3, V_2O_3, Cr_2O_3, and α-Fe_2O_3. Journal of Applied Physics, 50, 5285–5291.
Shannon, R.D. and Prewitt, C.T. (1970) Synthesis and structure of a new high-pressure form of Rh_2O_3. Journal of Solid State Chemistry, 2, 134–136.
Shim, S.-H., Duffy, T.S., and Shen, G. (2001) Stability and structure of $MgSiO_3$ perovskite to 2300 km depth of earth's mantle. Science, 293, 2437–2440.
Stacey, F.D. (1992) Physics of the earth. Brookfield Press, third edition.
Struzhkin, V.V., Goncharov, A.F., and Syassen, K. (1993a) Effect of pressure on magnetic excitations in CoO. Materials Science and Engineering A—Structural Materials Properties Microstructure and Processing, 168, 107–110.
Struzhkin, V.V., Schwarz, U., Wilhelm, H., and Syassen, K. (1993b) Effect of pressure on 2-magnon Raman scattering in K_2NiF_4. Materials Science and Engineering A—Structural Materials Properties Microstructure and Processing, 168, 103–106.
Suzuki, T., Yagi, T., Akimoto, S., Ito, A., Morimoto, S., and Syono, Y. (1985) X-ray diffraction and Mössbauer spectrum on the high pressure phase of Fe_2O_3. In S. Minomura Ed., Solid state physics under pressure, p. 149–154. Terra Scientific Publishing Company, Boston.
Ulbrich, H.H. and Waldbaum, D.R. (1976) Structural and other contributions to the third-law entropies of silicates. Geochimica et Cosmochimica Acta, 40, 1–24.
Wilburn, D.R. and Bassett, W.A. (1978) Hydrostatic compression of iron and related compounds: an overview. American Mineralogist, 63, 591–596.
Williams, Q., Jeanloz, R., and McMillan, P. (1987) Vibrational-spectrum of $MgSiO_3$ perovskite–zero-pressure Raman and midinfrared spectra to 27 GPa. Journal of Geophysical Research, 92, 8116–8128.
Xu, J.-A., Huang, E., Lin, J.-F., and Xu, L.Y. (1995) Raman study at high pressure and the thermodynamic properties of corundum: application of Kieffer's model. American Mineralogist, 80, 1157–1165.
Yagi, T. and Akimoto, S. (1982) Rapid X-ray measurements and static compression of α-Fe_2O_3. In S. Akimoto and M. H. Manghnani Eds., High-pressure research in geophysics, p. 81–90. Center for Academic Publications Japan, Tokyo.

MANUSCRIPT RECEIVED MARCH 28, 2001
MANUSCRIPT ACCEPTED NOVEMBER 7, 2001
MANUSCRIPT HANDLED BY CELIA MERZBACHER